RSC Advances

COMMUNICATION

View Article Online
View Journal | View Issue

Cite this: *RSC Adv.*, 2016, **6**, 96035

Received 17th July 2016
Accepted 26th September 2016

DOI: 10.1039/c6ra18188k

www.rsc.org/advances

In situ TEM observing structural transitions of MoS_2 upon sodium insertion and extraction†

Liqiang Zhang,‡[ab] Yushu Tang,‡[ab] Yuecun Wang,‡[c] Yongli Duan,[a] Degang Xie,[c] Chunyang Wu,[d] Lishan Cui,[ab] Yongfeng Li,*[a] Xiaohui Ning*[c] and Zhiwei Shan[c]

In this study, the sodiation and desodiation processes of MoS_2 were characterized by using an *in situ* TEM technique. The structural evolution of MoS_2 and its performance in a coin-type cell are recognized. Our findings provide a fundamental understanding of the reaction mechanism of MoS_2 as anode for Na ion batteries.

Recently, Na ion batteries (NIB) have been rapidly developed as an alternative to Li ion batteries (LIB) with an increasing number of experimental and theoretical studies.[1–6] As we know, the element Na is located next to Li among the alkali metals in the periodic table, and displays similar chemical actives as Li but with a much cheaper price and more abundant storage in nature.[7–9] Plenty of anode materials such as FeS_2, SnO_2, CuO and MoS_2 have been selected for NIBs, demonstrating good performances in experiments.[10–14] Among these promising anode materials, the layer structured material MoS_2 can accommodate guest ions intrinsically with a minimum structural distortion, which provides a good channel for the ions transportation. The weak interaction bonds between MoS_2 layers and larger interlayer spacing enables the Na ions insert and extract smoothly during cycling but without obviously volume expansion.[14] Previous studies have proposed that exfoliated MoS_2 nanosheet can operate stably in NIBs.[13,15,16] The crystalline structure evolution of MoS_2 upon sodiation is closely related to its electronic properties, which plays a significant role in determining the performance of the battery.[17] However, limited researches have been conducted on *in situ* characterizing and analyzing this process.

Understanding the detailed microscopic mechanisms of the electrochemical reaction and material degradation is crucial for the designing of high performance MoS_2 anodes for NIB. Thus in this work, an *in situ* transmission electron microscopy (TEM) technique has been applied to investigate the structural and chemical evolution of MoS_2 during Na ions insertion and desertion, providing a fundamental studying of the electrochemical reaction mechanism of MoS_2 as anode for NIBs.

The *in situ* electrochemical tests and TEM imaging were carried out by an *in situ* electric testing system, Hysitron PI95 H1H, inside the Hitachi H9500 TEM operated at 300 keV. In order to confirm the negligible effects of electron beam on electrochemical reactions, both beam-on and blank experiments were performed, respectively. The MoS_2 sample is prepared by means of supercritical CO_2 fluid shear, and the preparation progress is discussed in the ESI (Fig. S1†). A coin cell was also assembled to characterize the electrochemical performance of MoS_2 NIB. The electrochemical Na-storage properties of the MoS_2 were evaluated by galvanostatic cycling using CR2025-type coin cells. The cells were charged and discharged at various current densities between 0.005 and 3.0 V *vs.* Na/Na^+ on a Neware battery tester (Shenzhen, China). The specific capacity of MoS_2/G was calculated based on the total weight of MoS_2 and graphite. Cyclic voltammetry (CV) scanning was carried out on an Arbin BT2000 system between 0.005 and 3.0 V *vs.* Na/Na^+ at various scan rates using three-electrode beaker cells with Na foil as both the counter and reference electrodes. All of the electrochemical measurements were carried out at room temperature.

Here we examined the complete Na intercalation process in lamellar MoS_2 nanosheets *via* an *in situ* TEM approach to directly capture the dynamic changes. Fig. 1(a) shows a schematic illustration of the setup of MoS_2 NIBs. Metal Na serving as counter electrode is scratched by electrochemically shaped tungsten (W) tips. And the naturally grown sodium oxide and

[a]*State Key Laboratory of Heavy Oil Processing, China University of Petroleum, Changping, Beijing, 102249, China. E-mail: yfli@cup.edu.cn*

[b]*Department of Materials Science and Engineering, China University of Petroleum, Beijing 102249, China*

[c]*The Center for Advancing Materials Performance from the Nanoscale (CAMP-Nano), Xi An Jiao Tong University, Xian, 710049, China. E-mail: xiaohuining@mail.xjtu.edu.cn*

[d]*School of Materials Science and Engineering, Zhejiang University, Hangzhou, Zhejiang 310027, China*

† Electronic supplementary information (ESI) available: The preparation method of MoS_2 nanosheets; a schematic diagram of structure transformation of MoS_2; a cycling performance curve and a CV curve for Na/MoS_2 cell. See DOI: 10.1039/c6ra18188k

‡ These authors contributed equally to this work.

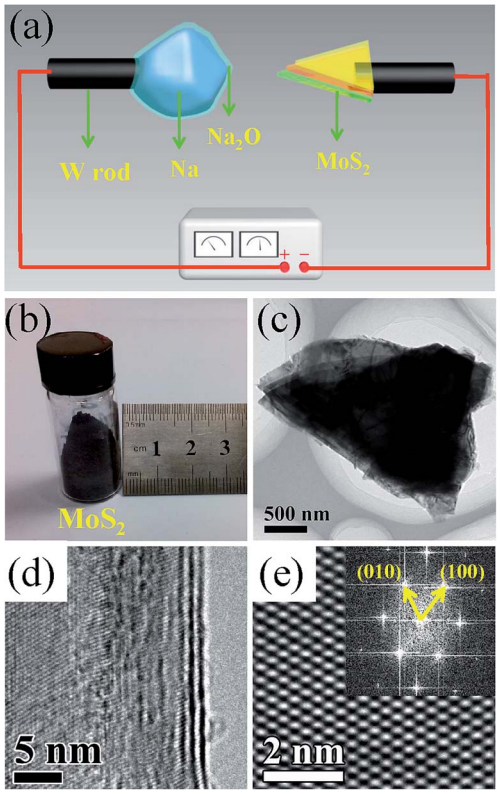

Fig. 1 (a) Schematic illustration of the setup of MoS_2/Na ion battery device. The MoS_2 nanosheet was cleaned and glued to a W rod using conducting epoxy. A bulk metal Na (cathode) was scratched on the surface of W tip. The natural generated Na_2O layer on the surface of metal Na was served as the solid electrolyte. (b) The photographs of the MoS_2. (c) A bright field TEM image of MoS_2 nanosheet. (d) A bright field TEM image showing the lamellar structure of MoS_2 nanosheet. (e) A HRTEM image of a MoS_2 nanosheet and the corresponding EDP shown in the upper inset.

hydroxide (Na_2O and NaOH) on the Na metal serve as a solid electrolyte. The lamellar MoS_2 electrodes were prepared by sticking a very thin sheet from the prepared MoS_2 nanosheet (Fig. 1(b)) to another W rod with conductive silver epoxy, these two electrodes are incorporated into the TEM specimen holder. Fig. 1(c) shows the TEM image for a MoS_2 nanosheet, which is thin enough to count its number of layer as shown in the HRTEM image (Fig. 1(d)). Fig. 1(e) shows the superstructure of MoS_2 nanosheet, and its corresponding electron diffraction pattern (EDP) is shown in the inset, which can be well indexed to the (010) and (100) planes of 2H-MoS_2 along the [001] zone axis (a = 3.16, JCPDF no. 06-0097).

Once the Na_2O-covered Na electrode driven by a piezoceramic manipulator was contacted to the MoS_2 nanosheet, a constant voltage was immediately applied on the sample to sodiate the MoS_2. The structural evolution of MoS_2 upon sodiation was recorded in Fig. 2(a–c), it shows that Na ions insert immediately into the space between the MoS_2 layers once the MoS_2 nanosheet attaches the metal Na electrode. When the reaction front is generated, it propagates extremely fast and sweeps across the MoS_2 sheet within a few seconds, as marked by the red arrows. The sodiated MoS_2 nanosheet can be separated into two segments

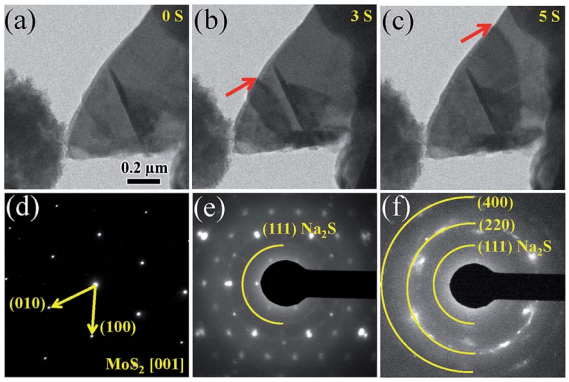

Fig. 2 *In situ* electrochemical reaction of lamellar MoS_2 nanosheets with Na. (a–c) A series of TEM images showing microstructural evolutions for a MoS_2 nanosheet during the first sodiation process. (d–f) *In situ* EDPs showing that MoS_2 was converted to Na_2S.

with different contrasts by the reaction fronts, corresponding to the pristine MoS_2 nanosheet on the right and the sodiated amorphous product on the left side, respectively. A real-time movie characterizing the first sodiation process is shown in ESI (movie S1†). The EDPs of the MoS_2 taken prior to, upon, and after the sodiation reaction are shown in Fig. 2(d–f), respectively. The pristine MoS_2 demonstrates obvious sharp Bragg spots in this EDP (Fig. 2(d)), indicating the single crystal structure of MoS_2. As the inserting of Na ions, those sharp spots become indistinct. Meanwhile some dim ones are generated between every two bright spots (forming a 2 × 2 superstructure). A typical structural transformation of MoS_2 from 2H to 1T is supposed to take place in this process (Fig. S2†), which is also observed upon the lithiation of MoS_2.[18] Meanwhile, some dim diffraction circles appear in Fig. 2(e) and the small circle near the center can be indexed to the (111) plane of Na_2S (JCPDF no. 03-0933) as marked by the yellow semicircle. It suggests that on this stage, a little amount of Na_2S has been generated in some part of the sodiation MoS_2 nanosheet. The sodiated structure has evolved into a 2 × 2 superstructure of Na_xMoS_2 mixing with a little amount of amorphous Na_2S. As the sodiation reaction goes on, more Na ions inserted into the MoS_2 nanosheets and the diffraction pattern changed from spots (Fig. 2(e)) into some brighter circles (Fig. 2(f)), which can be well indexed to the (111), (220) and (400) planes of Na_2S (JCPDF no. 03-0933). This change indicates that an amorphous Na_2S structure in the fully sodiated phase is formed, without any superstructure remaining, which means that the intercalation of more Na ions leads to lattice distortion of MoS_2 and formation of Na_2S. More Na ions insertion improve the bond formation between the Na and S atoms, which helps the formation of more Na_2S.[17] The reaction can be formulated as following equations:[18]

$$x\mathrm{Na} + 2\text{H-}\mathrm{MoS_2} \rightarrow 1\text{T-}\mathrm{Na_xMoS_2} \quad (1)$$

$$1\text{T-}\mathrm{Na_xMoS_2} + y\mathrm{Na^+} \rightarrow \mathrm{Na_2S} + \mathrm{Mo} \quad (2)$$

Noted that there is no diffraction pattern of Mo in Fig. 2(f). It is believed that the metallic Mo is well dispersed at the nanoscale level.[17]

Fig. 3 shows the microstructure evolutions of MoS_2 for the first sodiation and desodiation process. In Fig. 3(a–d), a nanoscale Na particle is gradually disappeared, indicating that the Na ions are inserting into the MoS_2 nanosheets. With a longer sodiation time, the lamellar MoS_2 becomes darker and darker as more Na ions are inserted. In Fig. 3(e–h), an obvious Na particle is generated on MoS_2 upon the desodiation and grows bigger within a few seconds, marked by the yellow arrows, indicating that Na ions are escaped from the sodiated MoS_2 rapidly. It is noted that Na can be easily squeezed out from the edge of the MoS_2 layers (as shown in ESI movie S2†) indicating that Na prefers to migrate along the edge of the MoS_2 nanosheets and the inserted Na ions could migrate smoothly between the MoS_2 layers. The *in situ* TEM patterns show that the lamellar structure of MoS_2 is stable during the sodiation and desodiation process without a significant volume expansion, and it confirms that MoS_2 nanosheet is an ideal anode material for the energy storage. Galvanostatic discharge–charge cycling is performed to directly measure the capacity of the MoS_2 electrode during sodiation and desodiation in a coin-type cell. The galvanostatic discharge–charge cycling is performed in a coin cell to directly measure the capacity of the MoS_2 electrode at a constant current rate of 200 mA g^{-1}. The cycling performance of the MoS_2 nanosheets is shown in Fig. S3.† The initial discharge and charge capacity is 175 and 167 mA h g^{-1} respectively. These capacities decrease gradually with the repeated cycling. This electrode shows stable cycling behavior for extended cycling period up to 50 cycles. Fig. S4† shows the cyclic voltammograms of the MoS_2 electrode at a scan rate of 0.2 mV s^{-1}. In the first discharging process, there exists two reduction peaks at 0.57 and 0.71 V in the potential range of 0.01–3 V. In the following charging process, four oxidation peaks appear at 1.33, 1.78, 2.28, and 2.52 V, indicating that MoS_2 undergoes multiphase conversions during cycling. The redox peaks decrease gradually during cycling corresponding to a slow degradation of charge–discharge capacities.[19] The above results indicate that MoS_2 anodes are ideal anode materials in practical NIBs. The MoS_2 nanosheets display no obvious changes in morphology during cycling, so they have a great potential to achieve long cycling lifetimes and good reversibility.

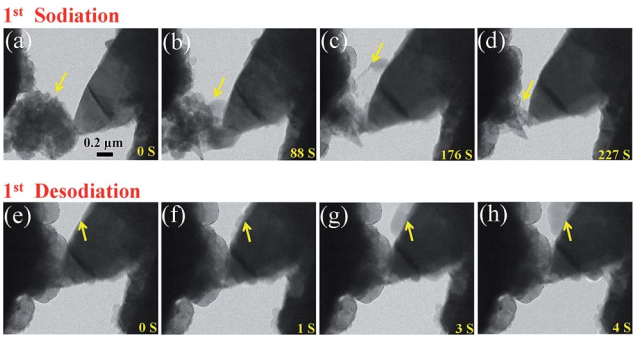

Fig. 3 Morphology evolutions of the MoS_2 nanosheet undergoing sodiation (a–d) and desodiation (e–h).

In conclusion, the detailed structure transformation of MoS_2 upon sodiation and desodiation processes have been characterized by using *in situ* TEM technique in this study. Upon the continuous sodiation of MoS_2, the pristine 2H-MoS_2 was first transformed to 1T-$NaMoS_2$ and finally converted into Na_2S phase. Meanwhile, the detailed microstructure evolution regarding the cycling process of MoS_2 nanosheets was also studied. The MoS_2 nanosheets assembled in a coin cell demonstrates a steady performance, indicating its layered structure provides an ideal channel for the Na ions migration in practical NIBs. These results provide important insights into understanding the mechanisms of structure evolution corresponding to the electrochemical property of MoS_2 during cycling.

Acknowledgements

This work was financially supported by the National Natural Science Foundation of China (No. 21322609, 21576289, 51401239, 51401157), Key Program Project of National Natural Science Foundation of China (51231008), Science Foundation of China University of Petroleum, Beijing (No. C201603, 2462014QZDX01, 2462015YQ0602), the National 973 program of China (2012CB619403) and Thousand Talents Program of China.

References

1 V. L. Chevrier and G. Ceder, *J. Electrochem. Soc.*, 2011, **158**, A1011.
2 F. Klein, B. Jache, A. Bhide and P. Adelhelm, *Phys. Chem. Chem. Phys.*, 2013, **15**, 15876–15887.
3 M. D. Slater, D. Kim, E. Lee and C. S. Johnson, *Adv. Funct. Mater.*, 2013, **23**, 947–958.
4 M. Gu, A. Kushima, Y. Shao, J.-G. Zhang, J. Liu, N. D. Browning, J. Li and C. Wang, *Nano Lett.*, 2013, **13**, 5203–5211.
5 Q. Su, G. Du, J. Zhang, Y. Zhong, B. Xu, Y. Yang, S. Neupane and W. Li, *ACS Nano*, 2014, **8**, 3620–3627.
6 D. Su and G. Wang, *ACS Nano*, 2013, **7**, 11218–11226.
7 Y. Wang, X. Yu, S. Xu, J. Bai, R. Xiao, Y.-S. Hu, H. Li, X.-Q. Yang, L. Chen and X. Huang, *Nat. Commun.*, 2013, **4**, 2365.
8 H. Zhu, Z. Jia, Y. Chen, N. Weadock, J. Wan, O. Vaaland, X. Han, T. Li and L. Hu, *Nano Lett.*, 2013, **13**, 3093–3100.
9 P. Senguttuvan, G. Rousse, M. E. Arroyo y de Dompablo, H. Vezin, J. M. Tarascon and M. R. Palacín, *J. Am. Chem. Soc.*, 2013, **135**, 3897–3903.
10 T. B. Kim, W. H. Jung, H. S. Ryu, K. W. Kim, J. H. Ahn, K. K. Cho, G. B. Cho, T. H. Nam, I. S. Ahn and H. J. Ahn, *J. Alloys Compd.*, 2008, **449**, 304–307.
11 L. Q. Zhang, X. H. Liu, Y. Liu, S. Huang, T. Zhu, L. J. Gui, S. X. Mao, Z. Z. Ye, C. M. Wang, J. P. Sullivan and J. Y. Huang, *ACS Nano*, 2011, **5**, 4800–4809.
12 L. Wang, K. Zhang, Z. Hu, W. Duan, F. Cheng and J. Chen, *Nano Res.*, 2014, **7**, 199–208.

13 G. S. Bang, K. W. Nam, J. Y. Kim, J. Shin, J. W. Choi and S.-Y. Choi, *ACS Appl. Mater. Interfaces*, 2014, **6**, 7084–7089.
14 L. David, R. Bhandavat and G. Singh, *ACS Nano*, 2014, **8**, 1759–1770.
15 C. Zhu, X. Mu, P. A. van Aken, Y. Yu and J. Maier, *Angew. Chem.*, 2014, **126**, 2184–2188.
16 M. Mortazavi, C. Wang, J. Deng, V. B. Shenoy and N. V. Medhekar, *J. Power Sources*, 2014, **268**, 279–286.
17 X. Wang, X. Shen, Z. Wang, R. Yu and L. Chen, *ACS Nano*, 2014, **8**, 11394–11400.
18 L. Wang, Z. Xu, W. Wang and X. Bai, *J. Am. Chem. Soc.*, 2014, **136**, 6693–6697.
19 J. Park, J.-S. Kim, J.-W. Park, T.-H. Nam, K.-W. Kim, J.-H. Ahn, G. Wang and H.-J. Ahn, *Electrochim. Acta*, 2013, **92**, 427–432.